Chinese Physics Letters

LETTER

Collective Dynamics of Nuclei from Quadrupole Splitting in an X-ray Cavity

Cite as: Xubo Liao *et al*. 2026 *Chin. Phys. Lett.* **43** 080101

DOI CSTR

Recommended Articles

Multi-Scale X-Ray Imaging Technologies for Rechargeable Batteries
Zihan Xu, Hanwen An, and Jiajun Wang
Chin. Phys. Lett. **41**, (2024)

Compression of Battery X-Ray Tomography Data with Machine Learning
Zipei Yan, Qiyu Wang, Xiqian Yu, Jizhou Li, and Michael K.-P. Ng
Chin. Phys. Lett. **41**, (2024)

Determine the Quantum Numbers of $X(6900)$ from Photon–Photon Fusion in Ultra-Peripheral Heavy Ion Collisions
Peng-Yu Niu, Yan-Chun Ding, Qian Wang, and Shuai Yang
Chin. Phys. Lett. **42**, 100202 (2025)

Magnetic Switching Dynamics and Tunnel Magnetoresistance Effect Based on Spin-Splitting Noncollinear Antiferromagnet Mn_3Pt
Meng Zhu, Jianting Dong, Xinlu Li, Fanxing Zheng, Ye Zhou, Kun Wu, and Jia Zhang
Chin. Phys. Lett. **41**, (2024)

Collective Pinning and Vortex Dynamics in Type II Superconducting Thin Films with Varying Magnetic Field at $T \to 0$
Yu Wu *et al*.
Chin. Phys. Lett. **42**, 100706 (2025)

Two Distinct Charge Orders in Infinite-Layer $PrNiO_{2+\delta}$ Revealed by Resonant X-Ray Diffraction
Xiaolin Ren *et al*.
Chin. Phys. Lett. **41**, 117404 (2024)

A series journal of Chinese Physical Society distributed by IOP Publishing

Chinese Physics Letters

Chin. Phys. Lett. **43** 080101 (2026)

LETTER

DOI: 10.1088/0256-307X/43/8/080101
CSTR: 32039.14.0256-307X.43.8.080101

Collective Dynamics of Nuclei from Quadrupole Splitting in an X-ray Cavity

Xubo Liao(廖旭波)[1,2,†], Yunyu Wang(王云宇)[1,2,†], Kangjun Xia(夏康俊)[1,2], Nan Xue(薛楠)[1,2], Xiangjin Kong(孔祥进)[1,2,*], and Yu-Gang Ma(马余刚)[1,2,3,*]

[1]Key Laboratory of Nuclear Physics and Ion-beam Application (MOE), Institute of Modern Physics, Fudan University, Shanghai 200433, China
[2]Research Center for Theoretical Nuclear Physics, NSFC and Fudan University, Shanghai 200438, China
[3]School of Physics, East China Normal University, Shanghai 200062, China

[†]These authors contributed equally to this work.
[*]Corresponding authors. Email: kongxiangjin@fudan.edu.cn; mayugang@fudan.edu.cn

Mössbauer nuclei with quadrupole-split levels provide a versatile platform for exploring coherent x-ray light-matter interactions. We theoretically study ensembles of ^{57}Fe nuclei embedded in thin-film x-ray cavities, explicitly accounting for different orientations of the electric field gradient. By mapping isotropic electric field gradient distributions to an effective equal-weight two-transition model, we derive analytical expressions for the time-dependent reflectivity and reveal the emergence of cavity-mediated quantum beats. The oscillation frequency and temporal profile of these beats can be tuned via the cavity-induced coherent coupling, offering a flexible approach to control collective nuclear dynamics and manipulate nuclear coherence in the x-ray regime.

Introduction

Mössbauer nuclei with extremely narrow resonances provide a unique platform for exploring coherent light–matter interactions in the x-ray regime [1−4]. The long nuclear coherence time enables collective phenomena such as superradiance [5] and cavity-modified spontaneous emission when the nuclei are embedded in thin-film x-ray cavities [6]. These features have established nuclear resonant scattering as a powerful setting for studying quantum optical effects at keV photon energies [7−12].

A key property of Mössbauer nuclei is the hyperfine interaction between the nuclear moments and their electromagnetic environment. Magnetic dipole and electric quadrupole interactions lift the degeneracy of nuclear levels and generate well-resolved hyperfine splittings, which determine the spectral structure and coherence dynamics of the nuclear ensemble [13−21]. In particular, quadrupole splitting arising from electric field gradient (EFG) in crystalline or layered materials introduces multiple transition channels with distinct energies and coupling strengths [22,23], providing an intrinsic handle for controlling collective nuclear dynamics [24].

When such hyperfine-structured nuclei are coupled to an x-ray cavity mode, the interplay between cavity-mediated collective excitation and quadrupole-induced level structure leads to rich dynamical behavior beyond that of an effective two-level system. Understanding how quadrupole splitting shapes the collective response is therefore essential for controlling nuclear coherence and engineering quantum optical functionality in the x-ray domain.

In this work, we investigate the collective dynamics of quadrupole-split Mössbauer nuclei embedded in an x-ray cavity while explicitly considering different orientations of the electric field gradient axis. We develop a theoretical model that incorporates the full hyperfine-resolved nuclear level structure. Based on this framework, we analyze the time-dependent nuclear response and demonstrate how the orientation of EFG axis governs the redistribution of excitation among the hyperfine transitions, leading to distinct features in the temporal emission from the cavity.

These results show that the quadrupole interaction provides an additional control parameter for shaping collective nuclear behavior in cavity-based x-ray quantum optics. Our findings contribute to a deeper understanding of hyperfine-structured nuclear ensembles in structured photonic environments and open new possibilities for manipulating nuclear coherence and time-domain responses through engineered electromagnetic surroundings.

Nuclear Level Schemes Under External Fields

We now investigate the influence of EFG in the ^{57}Fe Mössbauer ensemble. We consider an axially symmetric EFG, which arises from its surrounding electronic environment and couples to the nuclear quadrupole moment. This electric quadrupole interaction partially lifts the axial symmetry, leading to an energy splitting for the nuclear state with spin $I > 1/2$ given by [25]

$$E_m = 2\Delta_0 \frac{3m^2 - I(I+1)}{2I(2I-1)}, \tag{1}$$

where I is the nuclear spin, $m = -I, \ldots, I$ is the spin-projection quantum number, and $2\Delta_0$ denotes the total electric quadrupole splitting. For ^{57}Fe, the spins of the ground and excited states are $I_g = 1/2$ and $I_e = 3/2$, respectively. Thus, the quadrupole interaction splits the excited level into two twofold-degenerate sublevels: $|e_1\rangle$ with $m_e = \pm 3/2$ and $|e_2\rangle$ with $m_e = \pm 1/2$. The spin-(1/2) ground state $|g\rangle$ ($m_g = \pm 1/2$) remains degenerate.

For the 14.4 keV Mössbauer transition in ^{57}Fe [26], which has magnetic-dipole (M1) multipolarity, the allowed transitions satisfy the selection rule $M = m_e - m_g = 0, \pm 1$. The specific transition amplitudes depend on both the polarization and propagation direction of the incident x-ray pulse, as well as the direction of the EFG axis. We assume $\{\boldsymbol{e}_\sigma, \boldsymbol{e}_\pi, \boldsymbol{k}\}$ forms an orthonormal basis, where $\boldsymbol{k}$ denotes the wave vector of the incident x-ray pulse, and $\boldsymbol{e}_\sigma$ and $\boldsymbol{e}_\pi$ represent the two orthogonal polarization vectors, as shown in Fig. 1. The weight function of each resonant transition is given by the second-rank tensor [22]

$$\boldsymbol{W}_{m,m+M} = A \iint \sin\theta \mathrm{d}\theta \mathrm{d}\psi \; \boldsymbol{w}_{m,m+M}, \tag{2}$$

where A is the normalization factor. θ and ψ characterize the orientation of the EFG axis and satisfy $\cos\psi \sin\theta = \boldsymbol{f} \cdot \boldsymbol{e}_\sigma$, $\sin\psi \sin\theta = \boldsymbol{f} \cdot \boldsymbol{e}_\pi$,

Received 17 April 2026; accepted 11 July 2026; published 4 August 2026
© 2026 Chinese Physical Society and IOP Publishing Ltd. All rights, including for text and data mining, AI training, and similar technologies, are reserved.

Check for updates

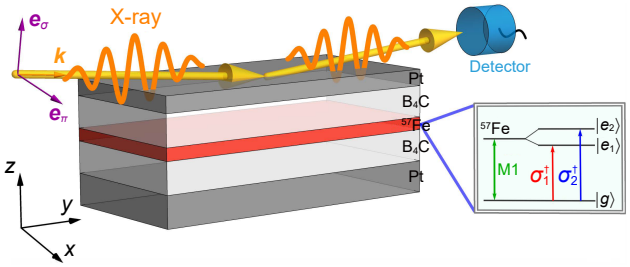

Fig. 1. Schematic of the x-ray thin-film cavity setup. The x-ray pulse is incident at a grazing angle, and the reflected signal is collected by a detector. The cavity is formed by a multilayer stack consisting of Pt(2.36 nm)/B_4C (3.45 nm)/^{57}Fe(1 nm)/B_4C(36.47 nm)/Pt(15.62 nm)/Al_2O_3. Inset: In the presence of the electric field gradient, the ^{57}Fe nucleus exhibits a three-level scheme.

and $\cos\theta = \boldsymbol{f}\cdot\boldsymbol{k}$, where $\boldsymbol{f}$ is the unit vector along EFG axis. Here, $\theta\in[0,\pi]$, $\psi\in[0,2\pi]$. $\boldsymbol{w}_{m,m+M}$ is the weight of transition at θ, ψ, and it takes the form [22]

$$\boldsymbol{w}_{m,m+M} = \frac{8\pi}{3}C^2(II'1;-m\ m+M)\boldsymbol{Y}^{(0)}_{1M}\otimes\boldsymbol{Y}^{(0)*}_{1M}. \tag{3}$$

Here, C is the Clebsch–Gordan coefficient [27], $\boldsymbol{Y}^{(0)}_{1M}$ is the vector spherical harmonic. The representation of $\boldsymbol{Y}^{(0)}_{1M}(\theta,\psi)$ in this basis is [22]

$$\begin{aligned}
\boldsymbol{Y}^{(0)}_{11} &= \sqrt{\frac{3}{16\pi}}[(-\cos\psi+\mathrm{i}\sin\psi\cos\theta)\boldsymbol{e}_\sigma-(\sin\psi+\mathrm{i}\cos\psi\cos\theta)\boldsymbol{e}_\pi],\\
\boldsymbol{Y}^{(0)}_{10} &= \mathrm{i}\sqrt{\frac{3}{8\pi}}\sin\theta(\sin\psi\boldsymbol{e}_\sigma+\cos\psi\boldsymbol{e}_\pi),\\
\boldsymbol{Y}^{(0)}_{1,-1} &= \sqrt{\frac{3}{16\pi}}[(\cos\psi+\mathrm{i}\sin\psi\cos\theta)\boldsymbol{e}_\sigma+(\sin\psi-\mathrm{i}\cos\psi\cos\theta)\boldsymbol{e}_\pi].
\end{aligned} \tag{4}$$

The detected intensity arises from the coherent sum of all individual contributions. In the following, we consider the case of a σ-polarized incident pulse.

Theoretical Methods

Next, we employ the quantum model developed in Refs. [28,29] to analyze the dynamics of a thin-film x-ray cavity containing resonant ^{57}Fe nuclei. The structure of the system is illustrated in Fig. 1. A σ-polarized x-ray pulse from a synchrotron radiation (SR) source is incident at a grazing angle φ_0. Due to the presence of EFG, each ^{57}Fe nucleus can be modeled as a three-level system: the two split excited states denoted by $|e_1\rangle$ and $|e_2\rangle$, and the ground state represented by $|g\rangle$. The two nuclear transitions are driven by the x-ray field with their respective dipole moments $\boldsymbol{d}_1$ and $\boldsymbol{d}_2$, where $\boldsymbol{d}_1$ and $\boldsymbol{d}_2$ denote the magnetic dipole moments associated with the M1 nuclear transition. They are determined by the reduced M1 matrix element together with the corresponding Clebsch–Gordan coefficient of the hyperfine transition. The ^{57}Fe nuclear ensemble is collectively coupled to the cavity field. By tracing out the photonic degrees of freedom, an effective nucleus-nucleus interaction Hamiltonian is derived as follows [28-32]

$$\begin{aligned}
\hat{H} = &-\sum_{i=1}^{N_\mu}\sum_{\mu=1}^{2}(\Delta+\Delta_\mu)\hat{\sigma}^\dagger_{i,\mu}\hat{\sigma}^-_{i,\mu}-\sum_{i=1}^{N_\mu}\sum_{j=1}^{N_\nu}\sum_{\mu,\nu=1}^{2}g_{\mu\nu}\hat{\sigma}^\dagger_{i,\mu}\hat{\sigma}^-_{j,\nu}\\
&-\sum_{i=1}^{N_\mu}\sum_{\mu=1}^{2}\left(\boldsymbol{d}^*_\mu\cdot\hat{\boldsymbol{E}}^+(\boldsymbol{r}_i)\hat{\sigma}^\dagger_{i,\mu}+\mathrm{h.c.}\right).
\end{aligned} \tag{5}$$

Here, $\hat{\sigma}^\dagger_{i,\mu}=|e_\mu\rangle\langle g|$ denotes the raising operator for the transition μ of the ith nucleus (with $\mu=1,2$), and N_μ is the number of nuclei contributing to transition μ. The detuning between the probe field and the nuclear transition is Δ, while Δ_μ characterizes the energy shift of the excited state $|e_\mu\rangle$. The second term in Eq. (5) describes effective dipole–dipole interactions mediated by the cavity, where $g_{\mu\nu}$ denotes the coupling strength. The third term represents the interaction between the nuclei and the probe field, with the Rabi frequency $\boldsymbol{d}^*_\mu\cdot\hat{\boldsymbol{E}}^+(\boldsymbol{r}_i)$, where $\hat{\boldsymbol{E}}^+(\boldsymbol{r}_i)$ denotes the amplitude of the probe field at the position $\boldsymbol{r}_i$ [28,29]. To eliminate the dependence on the transverse plane, we introduce the collective nuclear spin-wave operators [26]

$$\hat{S}_\mu = \sum_{i=1}^{N_\mu}\frac{1}{\sqrt{N_\mu}}\exp(-\mathrm{i}\boldsymbol{k}^{xy}\cdot\boldsymbol{r}_i^{xy})\hat{\sigma}^-_{i,\mu}, \tag{6}$$

where $\boldsymbol{k}^{xy}$ is the transversal component of the incident wave vector $\boldsymbol{k}$, $\boldsymbol{r}^{xy}$ denotes the coordinate of transversal plane. This spin-wave operator allows the Hamiltonian to be rewritten as

$$\hat{H} = -\sum_{\mu=1}^{2}(\Delta+\Delta_\mu)\hat{S}^\dagger_\mu\hat{S}_\mu-\sum_{\mu,\nu=1}^{2}J_{\mu\nu}\hat{S}^\dagger_\mu\hat{S}_\nu-\sum_{\mu=1}^{2}\left(\Omega_\mu\hat{S}^\dagger_\mu+\mathrm{h.c.}\right), \tag{7}$$

with the corresponding Lindblad operators [29]

$$\begin{aligned}
L[\hat{\rho}] = &-\sum_{\mu=1}^{2}\frac{\Gamma_0}{2}\left(\hat{S}^\dagger_\mu\hat{S}_\mu\hat{\rho}+\hat{\rho}\hat{S}^\dagger_\mu\hat{S}_\mu-2\hat{S}_\mu\hat{\rho}\hat{S}^\dagger_\mu\right)\\
&-\sum_{\mu,\nu=1}^{2}\frac{\Gamma_{\mu\nu}}{2}\left(\hat{S}^\dagger_\mu\hat{S}_\nu\hat{\rho}+\hat{\rho}\hat{S}^\dagger_\mu\hat{S}_\nu-2\hat{S}_\nu\hat{\rho}\hat{S}^\dagger_\mu\right).
\end{aligned} \tag{8}$$

Here, Γ_0 is the spontaneous decay rate of a single nucleus. The second term in $L[\hat{\rho}]$ describes the collective decay induced by the cavity. The quantities $J_{\mu\nu}$ and $\Gamma_{\mu\nu}$ are the coherent and incoherent coupling strengths between transitions, which are determined by the Green's function of the system $\boldsymbol{G}(\boldsymbol{r}_i,\boldsymbol{r}_j,\omega_\mathrm{p})$ and the number of nuclei N_μ, N_ν. Here, ω_p denotes the probe field. Ω_μ denotes the effective Rabi frequency for transition μ. By exploiting the translational invariance of our system in the (x,y) plane, the full Green's function can be expressed using a one-dimensional form $\boldsymbol{G}_{1D}(z_i,z_j,\omega_\mathrm{p},\boldsymbol{k}^{xy})$ [33]. Meanwhile, owing to the small thickness of the ^{57}Fe layer, we adopt the thin-layer approximation $\boldsymbol{G}_{1D}(z_i,z_j,\omega_\mathrm{p},\boldsymbol{k}^{xy})\simeq\boldsymbol{G}_{1D}(z_0,z_0,\omega_\mathrm{p},\boldsymbol{k}^{xy})$ for all i,j, yielding [29]

$$\begin{aligned}
J_{\mu\nu} &= \sqrt{N_\mu N_\nu}\frac{\mu_0\omega_\mathrm{p}^2}{D}\boldsymbol{d}^*_\mu\cdot\mathrm{Re}[\boldsymbol{G}_{1D}(z_0,z_0,\omega_\mathrm{p},\boldsymbol{k}^{xy})]\cdot\boldsymbol{d}_\nu,\\
\Gamma_{\mu\nu} &= \sqrt{N_\mu N_\nu}\frac{2\mu_0\omega_\mathrm{p}^2}{D}\boldsymbol{d}^*_\mu\cdot\mathrm{Im}[\boldsymbol{G}_{1D}(z_0,z_0,\omega_\mathrm{p},\boldsymbol{k}^{xy})]\cdot\boldsymbol{d}_\nu,
\end{aligned} \tag{9}$$

and

$$\Omega_\mu = \sqrt{N_\mu}\boldsymbol{d}^*_\mu\cdot\langle\hat{\boldsymbol{E}}^+_{1D}(z_0)\rangle, \tag{10}$$

where D is the transverse area defined in Ref. [28], $\hat{\boldsymbol{E}}^+_{1D}(z_0)$ denotes the field amplitude at position z_0. The dynamics of the full system is governed by the master equation [34]

$$\frac{\mathrm{d}}{\mathrm{d}t}\hat{\rho} = -\mathrm{i}[\hat{H},\hat{\rho}]+L[\hat{\rho}], \tag{11}$$

where $\hat{\rho}$ is the density matrix of the system. Using the input-output formalism [29]

$$\hat{\boldsymbol{E}}^+_{\mathrm{out}}(z) = \hat{\boldsymbol{E}}^+_{1D}(z)+\frac{\mu_0\omega_\mathrm{p}^2}{D}\sum_{\mu=1}^{2}\sqrt{N_\mu}\boldsymbol{G}_{1D}(z,z_0,\omega_\mathrm{p},\boldsymbol{k}^{xy})\cdot\boldsymbol{d}_\mu\hat{S}_\mu, \tag{12}$$

the reflectivity of the system can be obtained by

$$I = \left|\frac{\langle a_\mathrm{out}\rangle}{a_\mathrm{in}}\right|^2 = \left|\frac{\left\langle\hat{\boldsymbol{E}}^+_{\mathrm{out}}(z_\mathrm{top})\cdot\hat{\beta}\right\rangle}{a_\mathrm{in}}\right|^2, \tag{13}$$

where a_in stands for the input field, z_top is the top location, and $\hat{\beta}$ represents the polarization vector operator.

Different Orientations of EFG Axis

We now analyze the reflectivity spectrum in time domain under different orientations of EFG axis. Equations (2)–(4) indicate that the

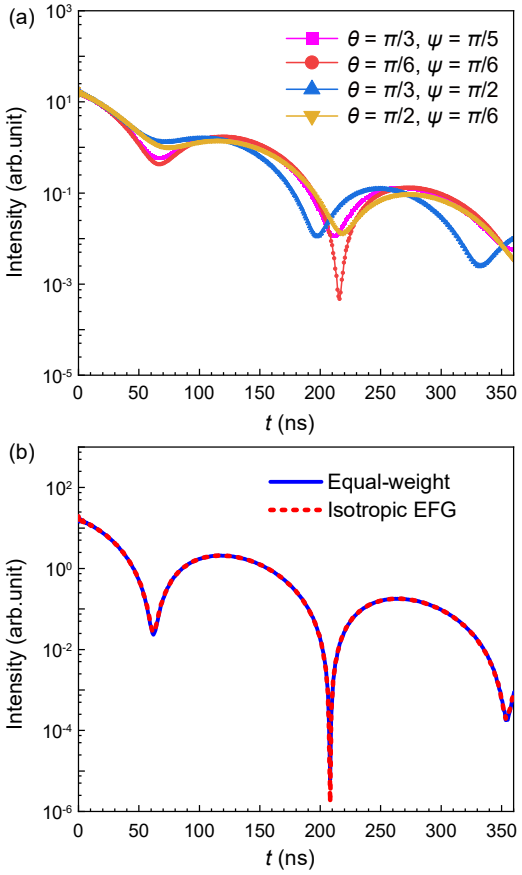

Fig. 2. Collective time dynamics of nuclei in the presence of quadrupole splitting in an x-ray cavity. (a) Time spectra for different orientations of the EFG axis. (b) Time spectra for the isotropic EFG distribution and for the equal-weight two-transition configuration.

orientation of the EFG axis primarily redistributes the transition amplitudes among different channels. In our system, the weight associated with each transition is proportional to $|\boldsymbol{d}|^2$ in Eq. (9). Therefore, variations in the transition weights directly affect both the coherent and incoherent coupling strengths between nuclei.

For the numerical calculations, we consider four representative orientations of the EFG axis: $\theta=\pi/3$, $\psi=\pi/5$; $\theta=\pi/6$, $\psi=\pi/6$; $\theta=\pi/3$, $\psi=\pi/2$; and $\theta=\pi/2$, $\psi=\pi/6$, with the quadrupole splitting set to $\Delta_0=3.1\Gamma_0$. The incident angle $\varphi_0=4220\,\mu\text{rad}$, corresponding to the fourth guided mode of the cavity. As shown in Fig. 2(a), pronounced quantum beats appear in the intensity reflectivity, with distinct oscillatory behaviors for different EFG-axis orientations. These results indicate that the orientation of the EFG axis significantly modifies the collective dynamics of nuclei in the cavity, even though the value of the quadrupole splitting remains unchanged. Moreover, the EFG-induced modulation mechanism is also expected to play a role in the presence of an external magnetic field, although the combined Zeeman and quadrupole interactions give rise to a more complex hyperfine structure and consequently different modulation behavior.

The Equivalence between Isotropic EFG and Equal-Weight Configuration

Next, we consider the special case of an isotropic EFG distribution which often occurs in crystallite samples. While a single EFG axis induces level splitting associated with two possible transitions, an isotropic distribution leads to a variety of transition configurations corresponding to different EFG-axis orientations. To describe this situation, we consider n uniformly distributed EFG axes, which induce $2n$ transitions with different weights.

Under this assumption, the Hamiltonian reads

$$\hat{H}=-\sum_{\mu=1}^{2n}\left(\Delta+\Delta_\mu\right)\hat{S}_\mu^\dagger\hat{S}_\mu-\sum_{\mu,\nu=1}^{2n}J_{\mu\nu}\hat{S}_\mu^\dagger\hat{S}_\nu-\sum_{\mu=1}^{2n}\left(\Omega_\mu\hat{S}_\mu^\dagger+\text{h.c.}\right), \tag{14}$$

where $\Delta_\mu=\pm\Delta_0$ corresponds to the energy shift of the two excited states, and $J_{\mu\nu}$ and Ω_μ take forms analogous to those in Eqs. (9) and (10). The Lindblad operators have the same structure as in Eq. (8),

$$\begin{aligned}L[\hat{\rho}]=&-\sum_{\mu=1}^{2n}\frac{\Gamma_0}{2}\left(\hat{S}_\mu^\dagger\hat{S}_\mu\hat{\rho}+\hat{\rho}\hat{S}_\mu^\dagger\hat{S}_\mu-2\hat{S}_\mu\hat{\rho}\hat{S}_\mu^\dagger\right)\\&-\sum_{\mu,\nu=1}^{2n}\frac{\Gamma_{\mu\nu}}{2}\left(\hat{S}_\mu^\dagger\hat{S}_\nu\hat{\rho}+\hat{\rho}\hat{S}_\mu^\dagger\hat{S}_\nu-2\hat{S}_\nu\hat{\rho}\hat{S}_\mu^\dagger\right).\end{aligned} \tag{15}$$

By numerical calculation, the time-dependent reflectivity is obtained and shown as the dashed line in Fig. 2(b). In the limit $n\to\infty$, the numerical result approaches that of a fully isotropic distribution. Furthermore, by summing the contributions of the two transitions over all EFG axes separately, the total weights of the two transitions are found to be equal [22]. Motivated by this result, we consider an effective level scheme consisting of two transitions with equal amplitude. The corresponding time response of this equal-weight configuration is shown by the solid line in Fig. 2(b). The two results agree excellently, demonstrating that the reflectivity spectrum obtained for the isotropic distribution coincides with that of the equal-weight configuration. Therefore, an isotropic EFG distribution can be accurately modeled by an effective equal-weight configuration with the same quadrupole splitting. This simplification greatly facilitates the calculations and enables an analytical treatment of the system dynamics under isotropic EFG distributions.

Derivation of the Time-Domain Reflectivity Formula for an Isotropic EFG Distribution

As discussed, an isotropic EFG distribution can be accurately modeled by an effective equal-weight configuration with the same quadrupole splitting. Based on this simplification, we derive the analytical expression of the reflectivity in the time domain using an effective equal-weight two-transition configuration. In the weak-excitation regime, the frequency-domain reflectivity can be written as

$$r=r_0+r_\text{N}=r_0+\frac{4\Omega^2\left(2\text{i}\Delta-\Gamma_0\right)}{\left(2\text{i}\Delta+4\text{i}J-\Gamma_0-2\Gamma\right)\left(2\text{i}\Delta-\Gamma_0\right)+4\Delta_0^2}, \tag{16}$$

where r_0 and r_N denote the responses of the empty cavity and the nuclear ensemble, respectively. Equation (16) exhibits two complex poles,

$$\Delta_\pm=-\frac{1}{2}\left[\text{i}(\Gamma+\Gamma_0)+2J\pm\sqrt{-(\Gamma-2\text{i}J)^2+4\Delta_0^2}\right], \tag{17}$$

corresponding to two eigenstates. The real and imaginary parts of $\Delta_\pm$ represent the resonant energies and linewidths of these states, respectively. Consequently, r_N can be expressed as a sum of two Lorentzian-like terms,

$$r_\text{N}=\frac{\alpha A_+}{\Delta-\Delta_+}+\frac{\alpha A_-}{\Delta-\Delta_-}, \tag{18}$$

where $\alpha=\Omega^2$, and the amplitude coefficients are $A_+=(\Gamma_0-2\text{i}\Delta_+)/(\Delta_+-\Delta_-)$ and $A_-=-(\Gamma_0-2\text{i}\Delta_-)/(\Delta_+-\Delta_-)$. To obtain the time-domain reflectivity, we apply the inverse Fourier transform,

$$r(t)=\frac{1}{2\pi}\int r(\Delta)\exp(-\text{i}\Delta t)\text{d}\Delta, \tag{19}$$

which yields

$$r(t)=r_0\delta(t)+\alpha\left[A_+\exp(-\text{i}\Delta_+t)+A_-\exp(-\text{i}\Delta_-t)\right]. \tag{20}$$

Here, $\delta(t)$ denotes the Dirac delta function, corresponding to the prompt reflection from the bare cavity, and the second term represents

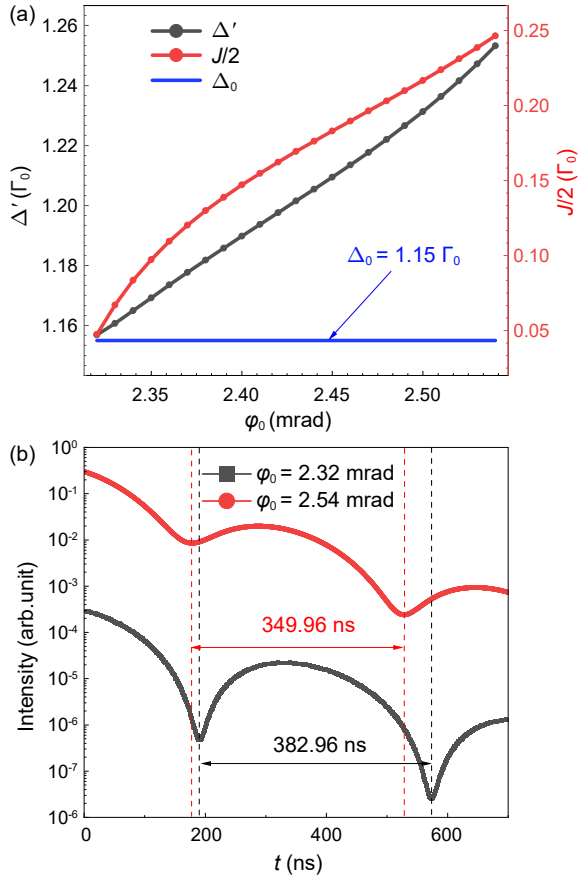

Fig. 3. (a) Frequency Δ' and strength $J/2$ as a function of incident angle φ_0, with $\varphi_0 \in [2.32, 2.54]$ mrad. The oscillation exhibits significant enhancement under the influence of J. The results are obtained for a quadrupole splitting of $\Delta_0 = 1.15\Gamma_0$. (b) The time-dependent intensity reflectivity under $\varphi_0 = 2.32$ mrad and 2.54 mrad.

the resonant response of the nuclear ensemble. The total reflectivity thus arises from the interference of the two resonant transitions, each characterized by its complex frequency and amplitude $A_\pm$.

Cavity-Mediated Quantum Beats Induced by An Isotropic Distribution of EFG

We now use the analytical expressions derived above to investigate the temporal reflectivity of the system under an isotropic EFG distribution. We focus on the regime where the coherent coupling J dominates over the incoherent decay Γ ($J \gg \Gamma$), which can be realized at specific incident angles φ_0. In this limit, the effect of Γ can be neglected to a good approximation. Under this assumption, the complex frequencies in Eq. (17) simplify to

$$\Delta_\pm = -\left[\mathrm{i}\frac{\Gamma+\Gamma_0}{2} + J \pm \sqrt{J^2+\Delta_0^2}\right]. \tag{21}$$

For convenience, we define $\Gamma' = (\Gamma+\Gamma_0)/2$ and $\Delta' = \sqrt{J^2+\Delta_0^2}$. The corresponding time-dependent intensity reflectivity is then

$$I_1(t) = |\alpha|^2 \exp(-2\Gamma' t)\left[2|A_+||A_-|\cos(2\Delta' t + \phi_c) + I_{\mathrm{const}}\right], \tag{22}$$

where ϕ_c denotes the constant phase difference between A_+ and A_-, $I_{\mathrm{const}} = |A_+|^2 + |A_-|^2$. This expression shows that the system exhibits quantum beats arising from the interference between the two transitions. The period of these cavity-mediated oscillations, $T_1 = \pi/\Delta'$, is shorter than the typical beat period $T_2 = \pi/\Delta_0$ observed for quadrupole splitting in free space. This reduction in period is a direct consequence of the coherent coupling J, which accelerates the oscillatory dynamics of the nuclear ensemble.

Figure 3(a) illustrates the angle-dependent oscillation frequency Δ' in the regime where $J \gg \Gamma$. To highlight the role of the coherent coupling, we set $\Delta_0 = 1.15\Gamma_0$. As φ_0 increases, the oscillation frequency grows significantly due to the enhancement of J, providing a practical mechanism to control the system dynamics.

Figure 3(b) shows two representative time-domain intensity traces corresponding to $\varphi_0 = 2.32$ mrad and $\varphi_0 = 2.54$ mrad. The difference in oscillation periods between these two angles exceeds 10 ns, demonstrating the tunability of quantum-beat dynamics via cavity-mediated coherent coupling. By adjusting the incident angle, one can effectively control both the frequency and temporal profile of the quantum beats, providing a flexible approach to manipulating collective nuclear dynamics in thin-film x-ray cavities.

Summary

We have studied the collective dynamics of quadrupole-split ^{57}Fe nuclei in thin-film x-ray cavities, highlighting the role of EFG orientation in shaping quantum beats. For isotropic EFG distributions, an effective equal-weight two-transition model accurately captures the nuclear response. In the regime $J \gg \Gamma$, cavity-mediated coherent coupling accelerates the oscillations, and the beat frequency can be tuned via the incident angle. These results demonstrate how quadrupole interactions combined with cavity effects enable control over collective nuclear coherence and time-domain dynamics, providing a route to engineer tailored x-ray quantum optical responses. Although the present work is restricted to the weak-excitation regime, additional calculations for a thin ^{57}Fe layer in free space indicate that the EFG-induced quantum-beat modulation remains robust beyond the weak-excitation regime, suggesting that the interplay between EFG-induced quantum interference and nonlinear nuclear dynamics may provide additional opportunities for controlling x-ray–nucleus interactions.

Acknowledgements

This work was supported by the National Key Research and Development Program of China (Grant No. 2024YFA1610900) and the National Natural Science Foundation of China (Grant Nos. 12447106, 12547102, and 12541501).

References

[1] Mössbauer R L 1959 *Z. Naturforsch. A* **14** 211
[2] Hannon J P and Trammell G T 1999 *Hyperfine Interact.* **123** 127
[3] Vagizov F G 1990 *Hyperfine Interact.* **61** 1359
[4] Adams B W, Buth C, Cavaletto S M, Evers J, Harman Z, Keitel C H, Pálffy A, Picón A, Röhlsberger R, Rostovtsev Y, and Tamasaku K 2013 *J. Mod. Optic.* **60** 2
[5] Röhlsberger R, Schlage K, Sahoo B, Couet S, and Rüffer R 2010 *Science* **328** 1248
[6] Röhlsberger R, Schlage K, Klein T, and Leupold O 2005 *Phys. Rev. Lett.* **95** 097601
[7] Röhlsberger R, Wille H, Schlage K, and Sahoo B 2012 *Nature* **482** 199
[8] Heeg K P, Wille H, Schlage K, Guryeva T, Schumacher D, Uschmann I, Schulze K S, Marx B, Kämpfer T, Paulus G G, Röhlsberger R, and Evers J 2013 *Phys. Rev. Lett.* **111** 073601
[9] Heeg K P, Haber J, Schumacher D, Bocklage L, Wille H, Schulze K S, Loetzsch R, Uschmann I, Paulus G G, Rüffer R, Röhlsberger R, and Evers J 2015 *Phys. Rev. Lett.* **114** 203601
[10] Heeg K P, Ott C, Schumacher D, Wille H, Röhlsberger R, Pfeifer T, and Evers J 2015 *Phys. Rev. Lett.* **114** 207401
[11] Haber J, Schulze K S, Schlage K, Loetzsch R, Bocklage L, Gurieva T, Bernhardt H, Wille H, Rüffer R, Uschmann I, Paulus G G, and Röhlsberger R 2016 *Nat. Photonics* **10** 445
[12] Haber J, Kong X, Strohm C, Willing S, Gollwitzer J, Bocklage L, Rüffer R, Pálffy A, and Röhlsberger R 2017 *Nat. Photonics* **11** 720
[13] Spijkerman J J, Travis J C, Pipkorn D N, and Violet C E 1971 *Phys. Rev. Lett.* **26** 323

[14] Wagner F E, Spieler H, Kucheida D, Kienle P, and Wäppling R 1972 *Z. Phys. A: Hadrons Nucl.* **254** 112
[15] Kistner O C and Sunyar A W 1960 *Phys. Rev. Lett.* **4** 412
[16] Matthias E, Schneider W, and Steffen R M 1962 *Phys. Rev.* **125** 261
[17] Cadogan J M and Ryan D H 2004 *Hyperfine Interact.* **153** 25
[18] Jerschow A 2005 *Prog. Nucl. Magn. Reson. Spectrosc.* **46** 63
[19] Nasu S 2013 *Mössbauer Spectroscopy: Tutorial Book* edited by Yoshida Y and Langouche G (Springer Berlin, Heidelberg)
[20] Heeg K P and Evers J 2013 *Phys. Rev. A: At. Mol. Opt. Phys.* **88** 043828
[21] Heeg K P and Evers J 2015 *Phys. Rev. A* **91** 063803
[22] Sturhahn W 2004 *J. Phys.: Condens. Matter* **16** S497
[23] Li Y, Wang Y, Zhao K, Ma Z, Wang Y, Yang Y, Kong X, Fu C, and Ma Y 2025 *Chin. Phys. Lett.* **42** 061201
[24] Wu L, Fu C, and Yan H 2025 *Chin. Phys. Lett.* **42** 120301
[25] Vij D R 2007 *Handbook of Applied Solid State Spectroscopy* (Springer Science & Business Media)
[26] Röhlsberger R 2005 *Nuclear Condensed Matter Physics with Synchrotron Radiation: Basic Principles, Methodology and Applications* (Springer Berlin, Heidelberg)
[27] Rose M E 1995 *Elementary Theory of Angular Momentum* (Courier Corporation)
[28] Lentrodt D, Heeg K P, Keitel C H, and Evers J 2020 *Phys. Rev. Res.* **2** 023396
[29] Kong X, Chang D E, and Pálffy A 2020 *Phys. Rev. A* **102** 033710
[30] Dung H T, Knöll L, and Welsch D G 2002 *Phys. Rev. A* **66** 063810
[31] Asenjo-Garcia A, Hood J D, Chang D E, and Kimble H J 2017 *Phys. Rev. A* **95** 033818
[32] Chang D E, Jiang L, Gorshkov A V, and Kimble H J 2012 *New J. Phys.* **14** 063003
[33] Tomaš M S 1995 *Phys. Rev. A* **51** 2545
[34] Scully M O and Zubairy M S 1997 *Quantum Optics* (Cambridge University Press)